metals

MDPI

Article

First-Principle Study on Tailoring the Martensitic Transformation of B2 $Nb_{50-x}Ti_xRu_{50}$ Shape-Memory Alloy for Structural Applications

Duduzile Nkomo [1,2,*], Yu-Nien Shen [3], Roelf Mostert [2], Yoko Yamabe-Mitarai [3,*] and Maje Phasha [1]

[1] Advanced Materials Division, Mintek, 200 Malibongwe Drive, Randburg 2125, South Africa; majep@mintek.co.za
[2] Department of Materials Science and Metallurgical Engineering, University of Pretoria, Hatfield, Pretoria 0028, South Africa; roelf.mostert@up.ac.za
[3] Department of Advanced Materials Science, University of Tokyo, 5-1-5 Kashiwanoha, Kashiwa-shi, Chiba 277-8561, Japan; 1140330566@edu.k.u-tokyo.ac.jp
* Correspondence: dudunk@mintek.co.za (D.N.); mitarai.yoko@edu.k.u-tokyo.ac.jp (Y.Y.-M.); Tel.: +27-011-709-4754 (D.N.); +81-4-7136-3783 (Y.Y.-M.)

Abstract: NbRu has a potential as a high-temperature shape-memory alloy (HTSMA) because it has a martensitic transformation temperature above 1000 °C. However, its shape-memory properties could be improved for consideration in the aerospace and automotive industry. The unsatisfactory shape-memory properties could be associated with the presence of a brittle tetragonal $L1_0$ martensitic phase. Therefore, in an attempt to modify the transformation path from B2→$L1_0$ in preference of either B2→orthorhombic or B2→monoclinic (MCL), an addition of B2 phase stabiliser, titanium (Ti), has been considered in this study to partially substitute niobium (Nb) atoms. The ab initio calculations have been conducted to investigate the effect of Ti addition on the thermodynamic, elastic, and electronic properties of the $Nb_{50-x}Ti_xRu_{50}$ in B2 and $L1_0$ phases. The results showed that the B2 and $L1_0$ phases had comparable stability with increasing Ti content. The simulated data presented here was sufficient for the selection of suitable compositions that would allow the $L1_0$ phase to be engineered out. The said composition was identified within 15–30 at.% Ti. These compositions have a potential to be considered when designing alloys for structural application at high temperatures above 200 °C.

Keywords: shape-memory alloy; alloy design; elastic properties; electronic structure; martensitic transformation; ab initio calculations; high-temperature shape-memory alloy

Citation: Nkomo, D.; Shen, Y.-N.; Mostert, R.; Yamabe-Mitarai, Y.; Phasha, M. First-Principle Study on Tailoring the Martensitic Transformation of B2 $Nb_{50-x}Ti_xRu_{50}$ Shape-Memory Alloy for Structural Applications. *Metals* **2024**, *14*, 976. https://doi.org/10.3390/met14090976

Academic Editor: Gabriel A. Lopez

Received: 23 July 2024
Revised: 21 August 2024
Accepted: 26 August 2024
Published: 28 August 2024

1. Introduction

Near-equiatomic NbRu compositions exhibit a cubic B2 phase structure above 1000 °C. During cooling below this temperature, the B2 structure transforms to a tetragonal $L1_0$ phase at ~1100 °C. Further cooling results in another phase transition from $L1_0$ to an MCL phase, starting at ~880 °C [1]. This high temperature of martensitic transformation renders this alloy a potential HTSMA. However, the shape-memory properties of NbRu are poor compared to those of the well-known TiNi [2–5]. Fonda et al. [1] investigated the shape-memory effect of NbRu by performing a bend test at 800 °C, which is in the $L1_0$ temperature region. It was observed that the test specimens were deformed to a greater extent, leading to cracking. Reheating the sample in the B2 region resulted in a fraction of cracks disappearing, which indicated the potential of this alloy to undergo shape recovery. However, the recovery ratio was very low. The cracking of the specimen is thought to have been due to one of the phases being brittle, thus leading to failure during bending. The recovery ratio of the $Nb_{50-x}Ru_{50+x}$ increased from 50% for $Nb_{50}Ru_{50}$ [1,6] to 88.9% for $Nb_{47}Ru_{53}$ [7], indicating the effect of the reduction of Nb.

The available phase diagram for NbRu shows that a decrease in Nb near-equiatomic compositions leads to promotion of MCL formation at a martensitic transformation temperature closer to 900 °C [1]. The MCL extends between 45–53 at.% Nb region on the phase diagram. Thus, it can be deduced that the previously observed recovery improvement upon the reduction of Nb may be attributed to the B2↔MCL reverse martensitic transformation. A similar martensitic transformation path is observed in TiNi, which is known to have a 100% recovery ratio. The understanding of the martensitic transformation path is important in the study of shape-memory properties. Since the NbRu near-equiatomic compositions involve the B2→$L1_0$→MCL, it seems the formation of a brittle $L1_0$ phase which forms easily due to slight tetragonal distortions of the B2 phase is detrimental to the shape-memory properties of this alloy. Therefore, it is of interest to study ways to avoid the formation of the tetragonal phase. At the moment, the promising way to achieve this is by aiming to reduce the Nb content [8,9].

Several studies have been dedicated to improving the shape-memory properties of the NbRu alloy. Chang-Long et al. [10] reported the thermodynamic properties of $Nb_{50-x}Ru_{50+x}$ using the first-principles method. It was noted that the B2 phase became less stable with decreasing Nb content below 50 at.%, indicating a decrease in the B2→$L1_0$ martensitic transformation temperature [10]. Additionally, Chang-Long et al. [11] further studied the impact of partially replacing Nb with Fe on the stability of B2 $Nb_{50-x}Fe_xRu_{50}$. The calculated heats of formation (HOF) showed the instability of the B2 phase as Fe was increased (decreasing Nb) [9]. In both instances, the results indicated that the dissolution of B2 into other phases decreases sharply as Nb is increased until a composition of 58 at.% is reached. Beyond this point, B2 becomes stable at room temperature [1]. However decreasing Nb below 54 at.% shifts the transformation path towards the B2→$L1_0$→MCL region, where the B2 phase is prone to atomic displacements and transformation. For example, in the Al-containing NbRu alloys with less than 50 at.% Nb, the $Nb_{34.99}Ru_{16.03}Al_{48.98}$ resulted in the formation of a hexagonal *C14* phase which was more stable than a B2 phase with an HOF value of −0.613 eV/atom. The $Nb_{22.93}Ru_{52.42}Al_{24.59}$ composition had an $L2_1$ cubic structure with an HOF of −0.666 eV/atom [12]. This proves that the reduction of Nb and it's substitution with a ternary element can supress the B2→$L1_0$ to below the critical temperature where a different phase is formed.

Although SME in NbRu alloys is associated with high-temperature $L1_0$→B2 phase transition, the tetragonal $L1_0$ martensitic phase has been found to have a high hardness of 715 HV. Similarly, the $L1_0$ phase is considered brittle in Co-Ni-Al alloy compared to the β phase and γ-phase, with 632 HV and 428 HV, respectively [13]. Moreover, the presence of a tetragonal $L1_0$ phase in Co-Ni-Ga alloys has been observed to decrease the compressive strain which leads to poor shape-memory properties and workability [14]. Other alloys, such as Ni-Tb-Mn-Ga [15], Ni-Mn-In [16], and (Ce,Y)-tetragonal Zr polycrystals [17], which contain tetragonal $L1_0$ martensite, have been found to have high hardness and elastic modulus, poor fracture toughness, and poor shape-memory effect.

The purpose of this study is, therefore, to suppress the formation of the $L1_0$ phase by substituting Nb with Ti. Most recently, ab initio calculations were used to generate elasticity data and showed that substituting Nb with Ti led to the predicted suppression of B2→$L1_0$, where the stability of the B2 phase was found to compete with the $L1_0$, which brought about the possibility that Ti addition may promote either B2→orthorhombic or B2→MCL [18]. In this work, the Nb atoms have been partially substituted by Ti and the effect thereof on the electronic properties of B2 and $L1_0$ NbRu phases is explored. Furthermore, the thermodynamic and elastic properties of the $L1_0$ phase have been investigated to establish whether the reduction of Nb composition by the addition of Ti can suppress B2→$L1_0$ in favour of either a B2→orthorhombic or B2→MCL transformation path.

2. Materials and Methods

All calculations in this study were performed using density functional theory (DFT)-based CASTEP code embedded in the Materials Studio 2020 software package [19]. Robust Vanderbilt ultrasoft pseudopotentials [20] were used to describe the ion–electron interaction within the generalised gradient approximation (GGA) [21] of Perdew–Burke–Ernzerhof (PBE) [22]. The crystal structures of a unit cell and 2 × 2 × 2 supercell of B2 phase with space group no. 221 Pm3m, consisting of 2 and 16 atoms, respectively, were built. Since the $L1_0$ phase results from slight tetragonal distortions of B2 phase, the crystal structure does not significantly differ visually; thus, the crystal models shown in Figure 1 represent both B2 and $L1_0$ phases of NbRu and $Nb_{50-x}Ti_xRu_{50}$. Convergence tests were conducted, and the system was found to converge at the cutoff energy of 700 eV and a k-point set of 16 × 16 × 16 and 8 × 8 × 8 for the unit cell and supercell, respectively. The effect of substituting Nb atoms with Ti atoms on the electronic properties was determined for the B2 phase to complement our previous work on the thermodynamic and elastic properties of the B2 structure [18]. The ternary compositions considered were of stoichiometry $Nb_{8-x}Ti_xRu_8$ (representing $Nb_{50-x}Ti_xRu_{50}$, spanning the entire composition range). In addition, the structural, thermodynamic, elastic, and electronic properties of the tetragonal $L1_0$ phase with space group no. 123 P4mmm (with similar compositions to those of B2) were calculated. The $L1_0$ systems were found to converge with an energy cutoff of 700 eV and the k-point set of 9 × 9 × 8 and 19 × 19 × 13 for a 2 × 2 × 2 supercell comprising 16 atoms and a unit cell, respectively. The lattice constants were calculated for a small strain of 0.004. All ground-state structures were optimised using the Broyden–Fletcher–Goldfarb–Shanno (BFGS) minimization scheme. The convergence criterion was set to the limit of 1×10^{-5} eV/atom. The maximum residual forces of 0.03 eV/Å, the maximum residual bulk stress of 0.05 GPa, and the maximum atomic displacement of 1×10^{-3} Å were utilised. Lattice dynamic properties such as phonon dispersion were calculated using a supercell defined by a cutoff radius of 3.5 Å employing the finite displacement supercell method within the code [23].

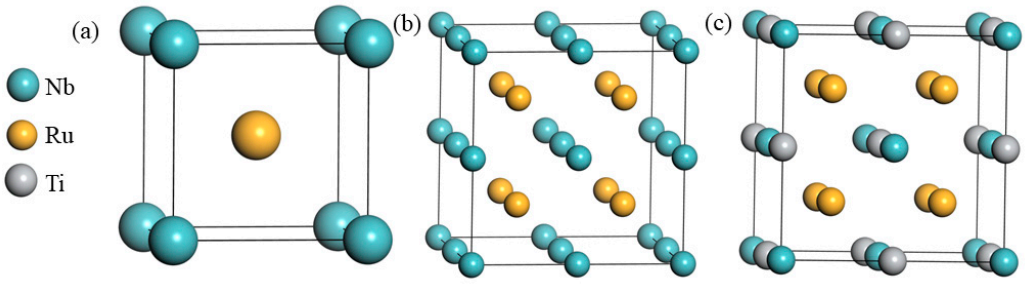

Figure 1. Crystal models representing B2 and $L1_0$: (**a**) unit cell, (**b**) 2 × 2 × 2 SC, and (**c**) 2 × 2 × 2 SC of $Nb_{50-x}Ti_xRu_{50}$ with Ti-occupied sites.

3. Results and Discussion

3.1. Lattice Parameters

Table 1 shows the previously calculated lattice parameters of the B2 phase [18] and the $L1_0$ phase. The values for lattice parameter a decrease with decreasing Nb content on the B2 phase, owing to Ti having a slightly smaller atomic radius than Nb and due to Nb having a larger thermal expansion compared to Ti. On the other hand, the lattice parameter $a = b$ value for $L1_0$ seems to increase with decreasing Nb content, reaches a maximum for $Nb_{25}Ti_{25}Ru_{50}$, and decreases further for the entire compositions, while the lattice parameter c decreases with increasing Ti content. The calculated lattice parameters for $L1_0$ deviate from the available experimental values by 1.54% percentage error for $a = b$ and by 3.56% for c [24]. These error margins are very likely to be accepted for computing crystal structure properties because they are less than 5%. The difference in the calculated values of lattice parameters a and c between those in the current study, the experimental value [24], theoretical value [25],and those reported in [6] may be attributed to the generated

convergence parameters. This effect of critically determining the convergence parameters has been discussed in our previous work [26], where poor selection of parameters may result in reporting of erroneous data because the structures are not fully converged and, thus, not fully optimised. The transformation from B2 to $L1_0$ is a result of Nb atoms shifting to preferentially occupy [1/2, 1/2, 1] octagonal sites along the *c*-axis; hence, the shift from ordered body-centred cubic (B2) lattice to body-centred tetragonal (bct) lattice with a tetragonal ratio $c/a > 1$ is observed. The calculated *c/a* ratio is presented in Table 1 below. The *c/a* ratio approaches 1 upon Ti addition, indicating that the B2 phase becomes more favourable than the $L1_0$ phase.

Table 1. Calculated lattice parameters for B2 and $L1_0$ phases of $Nb_{50-x}Ti_xRu_{50}$ (Å).

Alloy	B2 [18]	$L1_0$		
	a	**a = b**	**c**	**c/a**
$Nb_{50}Ru_{50}$	3.170 * 3.176 [24] 3.174 [10] 3.172 [27] 3.164 [25]	3.059 * 3.106 [24] 3.078 [6] 3.062 [25]	3.419 * 3.307 [24] 3.385 [6] 3.431 [25]	1.118 * 1.065 [24] 1.100 [6] 1.121 [25]
$Nb_{43.75}Ti_{6.25}Ru_{50}$	3.159	3.066	3.364	1.097
$Nb_{37.50}Ti_{12.50}Ru_{50}$	3.150	3.094	3.260	1.054
$Nb_{31.25}Ti_{18.75}Ru_{50}$	3.138	3.099	3.219	1.039
$Nb_{25}Ti_{25}Ru_{50}$	3.127	3.123	3.128	1.002
$Nb_{18.75}Ti_{31.25}Ru_{50}$	3.115	3.106	3.127	1.007
$Nb_{12.50}Ti_{37.50}Ru_{50}$	3.104	3.102	3.105	1.001
$Nb_{6.25}Ti_{43.75}Ru_{50}$	3.092	3.091	3.092	1.000
$Ti_{50}Ru_{50}$	3.080	3.080	3.081	1.000

* experimental.

3.2. Thermodynamic Stability

The thermodynamic stability for the B2 and $L1_0$ phases was determined by calculating the enthalpy (heat) of formation. The heat of formation (ΔH_f) is the amount of energy either absorbed or released during the formation of a compound and is calculated using the expression shown in Equation (1) for a constant pressure at $T = 0$ K. The more negative value of ΔH_f suggests that the structural phase is more thermodynamically stable. The heats of formation are presented in a graphical form in Figure 2 as a function of Ti content (x).

$$\Delta H_f = E_{Total} - \sum_i x_i E_i \quad (1)$$

where E_{Total} represents the total energy of the system, E_i is the total energies of the element i, and x_i is the concentration of element i in the compound in their respective ground-state structures.

As shown in Figure 2, the B2 phase is less thermodynamically stable at higher concentrations of Nb compared to $L1_0$. These results are in agreement with the available binary phase diagram of the NbRu which indicates that at 45 at.% Nb the B2→$L1_0$ phase transition is more thermodynamically favourable with a decrease in temperature. It is observed here that the addition of Ti increases the thermodynamic stability of the B2 phase, as demonstrated by the $\Delta H_f^{B2\text{-}L1_0}$ curve, with the most favourable composition to suppress the B2→$L1_0$ transformation being between 15 and 30 at.% Ti and the highest suppression expected at 25 at.% Ti. Beyond this composition range, the ΔH_f for both phases begins to equalize. $\Delta H_f^{B2\text{-}L1_0} = 0$ indicates that both phases have the same chance of forming. The current heat of formation data indicates that to avoid the formation of $L1_0$, Nb content must be decreased by Ti addition to stabilise B2 to about 900 °C, where the transformation to MCL starts to occur [1]. However, to identify a suitable composition for

suppression of $L1_0$ formation without compromising the martensitic transformation also requires consideration of elastic and electronic properties.

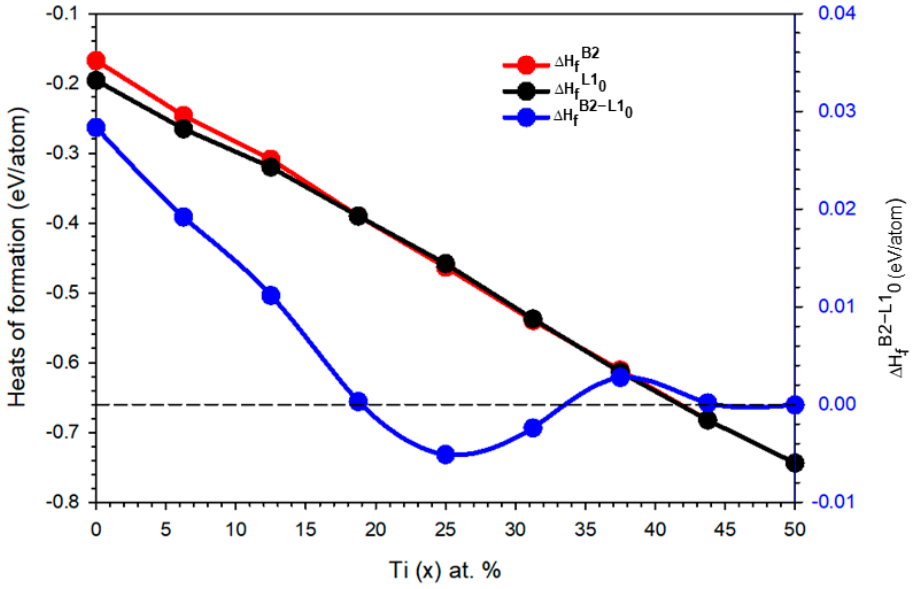

Figure 2. The theoretical HOF for B2, $L1_0$ $Nb_{50-x}Ti_xRu_{50}$, and $\Delta H_f^{B2\text{-}L1_0}$.

3.3. Elastic Properties

The mechanical stability condition of a lattice implies that the energy change $\Delta E \sim VC_{ije_ie_j}$, upon any small deformation, is positive. The mechanical stability criteria for the B2 phase were reported in our previous work [18]. In the cubic B2 lattice symmetry, there are three independent constants, which are C_{11}, C_{12} and C_{44}, of which the stability criteria are defined as $C_{11} - C_{12} > 0$ and $C_{44} > 0$. In a tetragonal $L1_0$ lattice symmetry, there are six independent elastic stiffness constants: C_{11}, C_{12}, C_{13}, C_{33}, C_{44}, and C_{66}. Therefore, the mechanical stability criteria for a tetragonal crystal are as follows: $C_{11} > |C_{12}|$, $C_{33} > 0$, $C_{44} > 0$, $C_{66} > 0$, $(C_{11} + C_{33} - 2C_{13}) > 0$ (denoted by C''), $(2C_{11} + C_{33} - 2C_{12} + 4C_{13}) > 0$ (denoted by C''') [28].

Table 2 shows the calculated elastic constants for the B2 and $L1_0$ phases. It is observed that the B2 phase meets the mechanical stability criteria, except for the first three Nb-rich compositions. On the other hand, the $L1_0$ phase shows mechanical stability and non-linearity as Ti content is increased, but the elastic constants are always positive.

Table 2. Elastic constants of B2 and $L1_0$ phases of $Nb_{50-x}Ti_xRu_{50}$ (GPa).

Alloy	B2 Elastic Constants [18]				$L1_0$ Elastic Constants								
	C_{11}	C_{12}	C_{44}	C'	C_{11}	C_{12}	C_{44}	C_{33}	C_{66}	C_{13}	C'	C''	C'''
$Nb_{50}Ru_{50}$	126	287	69	−81	328	204	46	341	58	178	103	310	1412
$Nb_{43.75}Ti_{6.25}Ru_{50}$	147	271	71	−62	363	150	68	323	64	177	107	333	1457
$Nb_{37.50}Ti_{12.50}Ru_{50}$	196	244	75	−24	318	177	73	245	68	212	70	138	1376
$Nb_{31.25}Ti_{18.75}Ru_{50}$	238	217	78	11	331	151	77	242	73	203	90	167	1414
$Nb_{25}Ti_{25}Ru_{50}$	274	178	80	48	296	195	83	290	83	196	50	195	1274
$Nb_{18.75}Ti_{31.25}Ru_{50}$	342	160	84	91	361	165	85	348	84	171	100	351	1429
$Nb_{12.50}Ti_{37.50}Ru_{50}$	396	133	87	132	398	130	87	405	88	132	133	521	1485
$Nb_{6.25}Ti_{43.75}Ru_{50}$	396	119	86	139	413	129	89	420	87	130	142	574	1506
$Ti_{50}Ru_{50}$	421	114	88	154	418	121	86	420	87	118	149	602	1488

To compare the mechanical stability of both phases, the tetragonal shear modulus C' for both phases has been calculated using the expression in Equation (2), and the values are presented in Table 2 and graphically depicted in Figure 3. The $L1_0$ phase has a more positive tetragonal shear modulus than the B2 phase, which means it is more mechanically stable than the B2 phase for most compositions but has lower C' values at 12.50 and 25 at.% Ti compositions. The decrease in C' for $L1_0$ may occur because at these compositions, the preferred structure is B2; thus, a reduction in mechanical stability takes place.

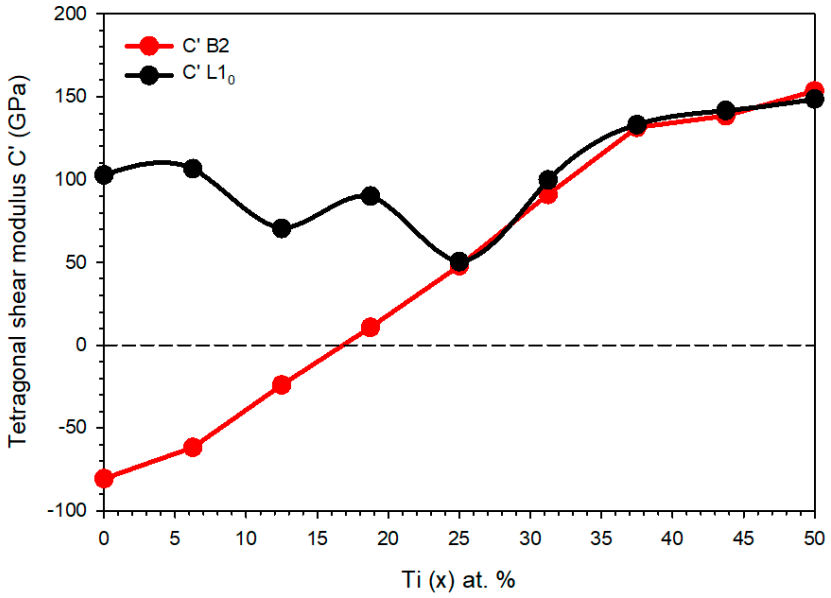

Figure 3. The tetragonal shear modulus C′ of B2 and $L1_0$ phases of $Nb_{50-x}Ti_xRu_{50}$.

Previously [18], we indicated that the suitable composition for further investigation of B2 alloys is where $C' \rightarrow 0$, which is between 12.50 and 18.75 at.% Ti. It is believed that the stress required to induce martensite at these compositions is small, and thus, the shape-memory properties could be improved. On the other hand, the current results show that the C' of the $L1_0$ phase remains positive but decreases with an increase in Ti composition, reaching a minimum at 25 at.% Ti. This further validates the claims that the limited shape-memory properties observed in NbRu arise due to the presence of this mechanically stable and brittle $L1_0$ phase which seems to compromise the possibility of further transition to the MCL phase.

$$C' = \frac{C_{11} - C_{12}}{2} \quad (2)$$

3.4. Electronic Properties

The electronic origin of the composition dependence on phase stability has been investigated and presented for all compositions in Figure 4, which shows the calculated total density of states (tDOS) of electrons for the B2 and $L1_0$ phases of $Nb_{50-x}Ti_xRu_{50}$ compositions. The tDOS can be used to predict the phase stability of a compound by observing the behaviour of energy states near the Fermi level ($E - E_f = 0$) concerning pseudogap. The Fermi level of the most stable structure can be indicated by the pseudogap being located in the deep valley, whereas the least stable structure has a Fermi level that lies at the shoulder or the peak. Also, if the DOS profiles and the Fermi level values for different structural phases are very similar due to the small energy difference, it means that there is a possibility for the co-existence of both phases [29].

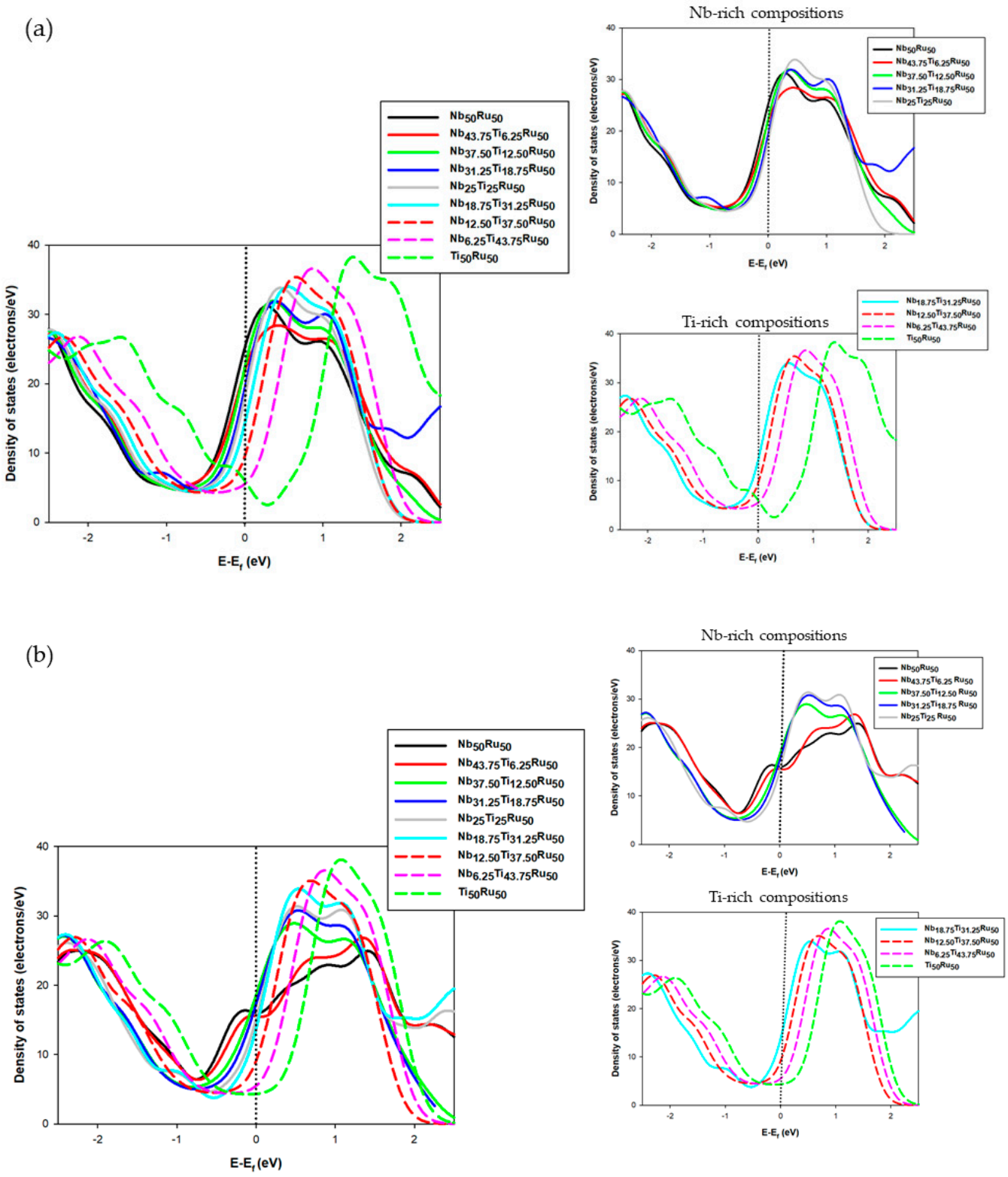

Figure 4. Total density of states (tDOS) of (**a**) B2 and (**b**) $L1_0$ $Nb_{50-x}Ti_xRu_{50}$.

The DOS around the Fermi level of $Nb_{50-x}Ti_xRu_{50}$ is mainly attributed to *d*-electrons of the constituent elements, with a small contribution from the *s*-orbital states. Figure 4a shows the B2 phase of $Nb_{50-x}Ti_xRu_{50}$. The Fermi level cuts the DOS curve at the shoulder, and the Fermi level seems to shift towards the centre of the pseudogap with increasing Ti content, indicating possible hybridisation between electronic *d*-orbitals. These *d*-*d* interactions are

known to form tight bonds and thus exert strong *d-d* electron interactions; hence, the electrons are transferred to a lower energy range and a pseudogap is produced. This is why the B2 phase becomes more stable as Ti content increases. This indicates that the high symmetry B2 phase of Nb-rich alloys cannot maintain the ordered structure at low temperatures; thus, they readily undergo martensitic transformation to the $L1_0$ phase.

On the other hand, Figure 4b shows the tDOS for the $L1_0$ $Nb_{50-x}Ti_xRu_{50}$. Similar to the B2 phase, the stability of the $L1_0$ phase seems to improve with increasing Ti content. This agrees well with the experimental data, as $Nb_{50}Ru_{50}$ has been found to have a high transformation temperature, meaning that it undergoes structural reconfiguration from B2→$L1_0$. For the Ti-rich systems, it appears that the $L1_0$ phase follows similar DOS profiles and Fermi level values as those of B2 structures, implying that both phases are likely to occur at T = 0 K, as was earlier demonstrated by the calculated heats of formation.

3.5. Lattice Dynamics

Figure 5a,b show the analysis of vibrational properties of the B2 and $L1_0$ phases of $Nb_{50-x}Ti_xRu_{50}$ as a function of Ti concerning the phonon dispersions at 0K. For B2 $Nb_{50-x}Ti_xRu_{50}$ shown in Figure 5a, the lattice vibrations revealed negative imaginary frequencies along X-R, R-M, G-M, and G-R high-symmetry directions of the Brillouin zone (BZ). Negative frequencies indicate that the B2 phase of NbRu is vibrationally unstable at 0K, confirming that it is a high-temperature phase likely to martensitically transform to another phase upon cooling. The atomic vibrations are stronger along the G-R direction, corresponding to the [111] direction on the lattice, which is predicted to be responsible for the formation of the trigonal *R3M* phase with space group no. 160, whilst the negative frequencies along the R-M direction are associated with the formation of the tetragonal phase. As the Ti content is increased, the vibrations along the R direction intensify until $Nb_{31.25}Ti_{12.50}Ru_{50}$ but weaken afterwards. These vibrations correspond to the [111] direction of the lattice, which is responsible for the transformation of B2 to an MCL phase variant. The soft modes along G-R disappear as Ti is increased towards 25 at.%, where only positive frequencies are observed, indicating that the B2 structure becomes more stable as Ti is increased.

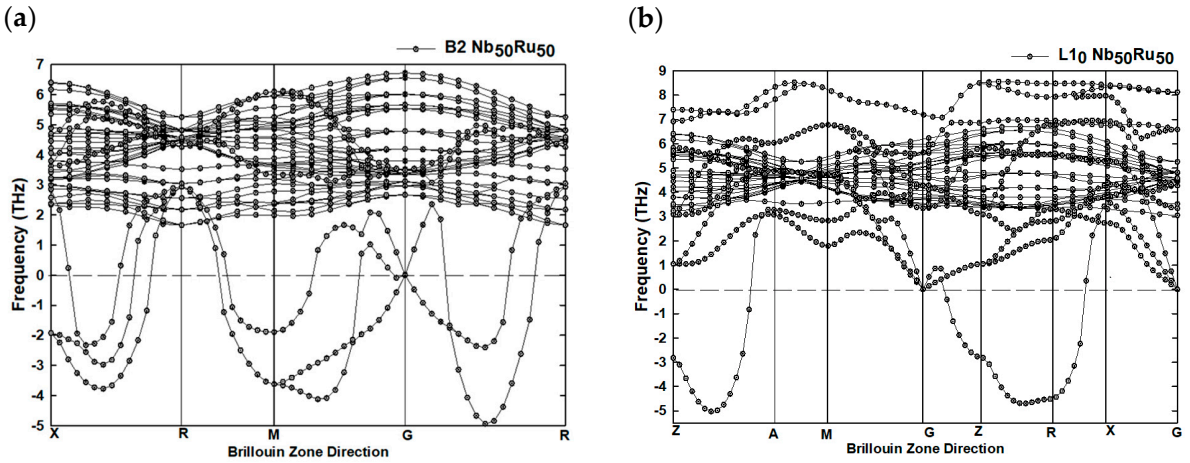

Figure 5. *Cont.*

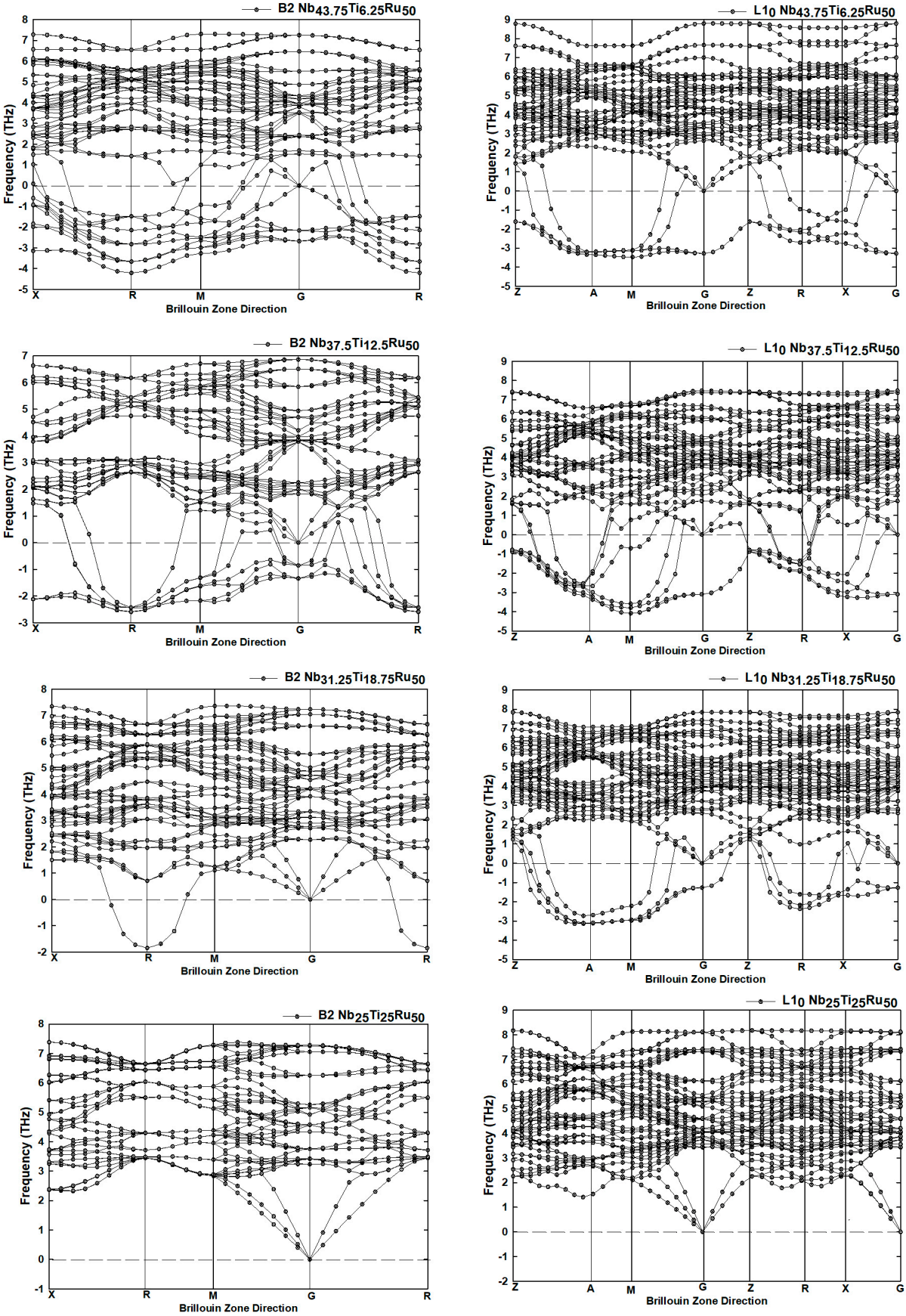

Figure 5. Phonon dispersion curves of (**a**) B2 and (**b**) $L1_0$ phases of $Nb_{50-x}Ti_xRu_{50}$ ($0 \leq x \leq 25$).

Similarly, the vibrational stability of the $L1_0$ phase of NbRu showed negative frequencies along the Z-A, G-Z, Z-R, and R-X directions of the Brillouin zone, representing [110], [001], and [010] respective directions of the $L1_0$ lattice structure. These vibrations are associated with the formation of a different variant of tetragonal structure with a space group no. 99 (*P4MM*) along [001], whilst the vibrations along the [110] direction are associated with the transformation to orthorhombic symmetry with space group no. 38 (*AMM2*); for the Z-R direction, the vibrations along the [010] direction of the lattice lead to the formation of an orthorhombic phase with symmetry space group no. 25 (*PMM2*). The displayed frequencies are indicative of the further transformation of the $L1_0$ phase. As the Ti content increases, the negative frequencies are intensified along the A-M and M-G directions, which corresponds to the [001] and [110] direction on the $L1_0$ lattice structure. Atomic displacement along these directions indicates that the $L1_0$ symmetry is maintained or the transformation to an orthorhombic phase is likely to occur as Ti is increased. The negative frequencies disappear on the $Nb_{25}Ti_{25}Ru_{50}$, meaning that the $L1_0$ phase becomes stable with no possibility of further martensitic transformation. Although $L1_0 \rightarrow$MCL has been reported previously [24,25], there are still debates about the actual structure of the low-temperature phase of NbRu regarding whether it is orthorhombic or monoclinic. However, this is beyond the scope of the current paper. The results shown on the dispersion curves, therefore, predict that the stability of both the B2 and $L1_0$ phases is almost the same within the considered compositions. However, the composition where the vibrations along the [111] direction are intensified corresponds to the transformation path alteration to possible B2→orthorhombic or B2→MCL transformations that are of interest, i.e., between 12.50 at.% and 18.75 at.% Ti.

4. Potential Applications of Ti Containing NbRu Alloys

It has been established that NbRu exhibits high martensitic temperature above 1000 °C. However, the martensite formed at this temperature is brittle. In a quest to improve its mechanical properties, Ti has been considered because it is lighter and has good corrosion resistance, making it suitable for structural applications above 200 °C. There is a threshold with adding Ti because it decreases the martensitic transformation to below 1000 °C. The engineering-out of the brittle $L1_0$ phase entails that the new transformation temperature will be below 800 °C. At this temperature, Ti-containing NbRu will still be considered the HTSMA. Therefore, the proposed alloy may find application in designing materials with high damping capacity for turbomachinery rotor blades operating at temperatures around 300 °C, with a high structural loss factor of at least 0.18 [30]. Furthermore, the alloy could be used for designing actuating materials in aeronautics, such as aircraft wing box structure reinforcements and fuselage structures [31,32], and in aerospace propulsion, with transformation temperatures ranging between 200–1000 °C [32–34].

5. Conclusions

The structural, thermodynamic, elastic, and electronic properties of the B2 and $L1_0$ phases have been investigated and reported in this study. This study aimed to predict a composition range within which potential HTSMA NbRu shape-memory properties can be improved by avoiding the B2→$L1_0$ and facilitating either the B2→orthorhombic or B2→MCL martensitic transformation. This was achieved by the systematic addition of Ti as a substitute at the Nb sites. The DFT method was then used to generate thermodynamic and mechanical stability data for both B2 and $L1_0$. The results from calculated HOF and elasticity data indicated that the addition of Ti improves both stabilities of the B2 and $L1_0$ phases. Thus, properties investigated in this work suggest that Ti compositions between 15 and 25 at.% are worth exploring experimentally in an attempt to improve the shape-memory properties of B2 NbRu for HTSMA applications. This work further predicts that it is possible to suppress B2→$L1_0$ in favour of either a B2→orthorhombic or B2→MCL martensitic transformation path by substitutional replacement of Nb atoms by Ti atoms. The likelihood of the latter will be considered in future work.

Author Contributions: Conceptualization, M.P., R.M. and Y.Y.-M.; methodology, D.N., Y.-N.S. and R.M.; software, D.N. and M.P.; validation, M.P.; formal analysis, D.N. and R.M.; investigation, D.N. and R.M.; resources, M.P., R.M. and Y.Y.-M.; data curation, D.N. and Y.-N.S.; writing—original draft preparation, D.N.; writing—review and editing, D.N., M.P., Y.Y.-M. and R.M.; visualization, D.N.; supervision, M.P., R.M. and Y.Y.-M.; project administration, M.P., R.M. and D.N.; funding acquisition, M.P. All authors have read and agreed to the published version of the manuscript.

Funding: This research was funded by Advanced Metals Initiative (AMI) of the Department of Science and Innovation (DSI), as well as the National Research Foundation (NRF) South Africa—JSPS [GRANT No: 148782] for financial support. Gratitude is also extended to the Centre for High-Performance Computing (CHPC) in Cape Town for allowing us to carry out the calculations using their remote computing resources.

Data Availability Statement: The raw data supporting the conclusions of this article will be made available by the authors on request.

Conflicts of Interest: The authors declare no conflicts of interest.

References

1. Fonda, R.; Jones, H.; Vandermeer, R. The shape memory effect in equiatomic TaRu and NbRu alloys. *Scr. Mater.* **1998**, *39*, 1031–1037. [CrossRef]
2. Cai, W.; Zheng, Y.F.; Meng, X.; Zhao, L.C. Superelasticity in TiNi Alloys and Its Applications in Smart Systems. *Mater. Sci. Forum* **2005**, *475–479*, 1915–1920. [CrossRef]
3. Otsuka, K.; Ren, X. Physical metallurgy of Ti–Ni-based shape memory alloys. *Prog. Mater. Sci.* **2005**, *50*, 511–678. [CrossRef]
4. Huang, X.; Ackland, G.J.; Rabe, K.M. Crystal structures and shape-memory behaviour of NiTi. *Nat. Mater.* **2003**, *2*, 307–311. [CrossRef] [PubMed]
5. Ye, Y.Y.; Chan, C.T.; Ho, K.M. Structural and electronic properties of the martensitic alloys TiNi, TiPd, and TiPt. *Phys. Rev. B* **1997**, *56*, 3678–3689. [CrossRef]
6. Firstov, G.S.; Kosorukova, T.A.; Koval, Y.N.; Verhovlyuk, P.A. Directions for High-Temperature Shape Memory Alloys' Improvement: Straight Way to High-Entropy Materials? *Shape Mem. Superelasticity* **2015**, *1*, 400–407. [CrossRef]
7. Tan, C.; Cai, W.; Tian, X. Structural, electronic and elastic properties of NbRu high-temperature shape memory alloys. *Scr. Mater.* **2007**, *56*, 625–628. [CrossRef]
8. Manzoni, A.; Chastaing, K.; Denquin, A.; Vermaut, P.; Portier, R. Phase transformation and shape memory effect in Ru-based high temperature shape memory alloys. *Solid State Phenom.* **2011**, *172–174*, 43–48. [CrossRef]
9. Chastaing, K.; Denquin, A.; Portier, R.; Vermaut, P. High-temperature shape memory alloys based on the RuNb system. *Mater. Sci. Eng. A* **2008**, *481–482*, 702–706. [CrossRef]
10. Chang-Long, T.; Wei, C.; Xiao-Hua, T. Combined experimental and theoretical study on the effect of Nb content on martensitic transformation of NbRu shape memory alloys. *Chin. Phys. B* **2010**, *19*, 430–435. [CrossRef]
11. Chang-Long, T.; Xiao-Hua, T.; Wei, C. Effect of Fe on martensitic transformation of NbRu high-temperature shape memory alloys: Experimental and theoretical study. *Chin. Phys. Lett.* **2008**, *25*, 3372–3374. [CrossRef]
12. Benarchid, M.; David, N.; Fiorani, J.-M.; Vilasi, M.; Benlaharche, T. Enthalpies of formation of Nb–Ru and Nb–Ru–Al alloys. *Thermochim. Acta* **2009**, *482*, 39–41. [CrossRef]
13. Ju, J.; Liu, H.; Shuai, L.; Liu, Z.; Kang, Y.; Yan, C.; Li, H. Martensite Transformation and mechanical properties of polycrystalline Co-Ni-Al alloys with Gd doping. *Metals* **2018**, *8*, 848. [CrossRef]
14. Li, Y.; Xin, Y.; Chai, L.; Ma, Y.; Xu, H. Microstructures and shape memory characteristics of dual-phase Co–Ni–Ga high-temperature shape memory alloys. *Acta Mater.* **2010**, *58*, 3655–3663. [CrossRef]
15. Wu, Y.; Wang, J.; Jiang, C.; Xu, H. Martensitic transformation, shape memory effect and mechanical properties of dual-phase $Ni_{50-x}Tb_xMn_{30}Ga_{20}$ (x = 0–1) alloys. *Mater. Sci. Eng. A* **2015**, *646*, 288–293. [CrossRef]
16. Zhou, L.; Mehta, A.; Giri, A.; Cho, K.; Sohn, Y. Martensitic transformation and mechanical properties of $Ni_{49+x}Mn_{36-x}In_{15}$ (x = 0, 0.5, 1.0, 1.5 and 2.0) alloys. *Mater. Sci. Eng. A* **2015**, *646*, 57–65. [CrossRef]
17. Hayakawa, M.; Inoue, Y.; Oka, M.; Nakagawa, H. Martensitic Transformation and Mechanical Properties of (Y, Ce)-Tetragonal Zirconia Polycrystals. *Mater. Trans. JIM* **1995**, *36*, 729–734. [CrossRef]
18. Nkomo, D.; Khodja, M.; Moller, H.; Phasha, M. The effect of systematic substitution of Nb with Ti on a potential high-temperature shape memory alloy: B2 NbRu. *MATEC Web Conf.* **2023**, *388*, 07018. [CrossRef]
19. Clark, S.J.; Segall, M.D.; Pickard, C.J.; Hasnip, P.J.; Probert, M.I.J.; Refson, K.; Payne, M.C. First principles methods using CASTEP. *Z. Kristallogr.* **2005**, *220*, 567–570. [CrossRef]
20. Vanderbilt, D. Soft self-consistent pseudopotentials in a generalized eigenvalue formalism. *Phys. Rev. B* **1990**, *41*, 7892–7895. [CrossRef]
21. Perdew, J.P.; Wang, Y. Accurate and simple analytic representation of the electron-gas correlation energy. *Phys. Rev. B* **1992**, *45*, 13244. [CrossRef] [PubMed]

22. Perdew, J.P.; Burke, K.; Ernzerhof, M. Generalized gradient approximation made simple. *Phys. Rev. Lett.* **1996**, *77*, 3865–3868. [CrossRef] [PubMed]
23. Hadi, M.A.; Christopoulos, S.-R.G.; Chroneos, A.; Naqib, S.H.; Islam, A.K.M.A. DFT insights into the electronic structure, mechanical behaviour, lattice dynamics and defect processes in the first Sc-based MAX phase Sc_2SnC. *Sci. Rep.* **2022**, *12*, 14037. [CrossRef] [PubMed]
24. Shapiro, S.M.; Xu, G.; Gu, G.; Gardner, J.; Fonda, R.W. Lattice dynamics of the high temperature shape memory alloy Nb-Ru. *Phys. Rev. B* **2006**, *73*, 214114. [CrossRef]
25. Chen, W.; Yuan, R.; Tan, F.; Xu, W. First-principles determination of the crystallography of the low-temperature phase for NbRu and TaRu shape memory alloys. *Phys. Chem. Chem. Phys.* **2022**, *24*, 22599–22604. [CrossRef] [PubMed]
26. Nkomo, D.; Ngobe, B.; Phasha, M.; Yamabe-Mitarai, Y. The SCF convergence criteria of the ab initio calculations of elastic properties of single-crystal B2 ZrPd phase. *Mater. Today Proc.* **2023**, *in press*. [CrossRef]
27. Mousa, A.A.; Hamad, B.A.; Khalifeh, J.M. Structure, electronic and elastic properties of the NbRu shape memory alloys. *Eur. Phys. J. B* **2009**, *72*, 575–581. [CrossRef]
28. Grimvall, G.; Magyari-Köpe, B.; Ozoliņš, V.; Persson, K.A. Lattice instabilities in metallic elements. *Rev. Mod. Phys.* **2012**, *84*, 945–986. [CrossRef]
29. Chen, X.-Q.; Fu, C.; Morris, J.R. The electronic, elastic, and structural properties of Ti–Pd intermetallics and associated hydrides from first principles calculations. *Intermetallics* **2010**, *18*, 998–1006. [CrossRef]
30. Duffy, K.P.; Padula, S.A., II; Scheiman, D.A. Damping of high-temperature shape memory alloys. *Behav. Mech. Multifunct. Compos. Mater.* **2008**, *6929*, 69291C. [CrossRef]
31. Padula, S.; Bigelow, G.; Noebe, R.; Gaydosh, D.; Garg, A. Challenges and progress in the development of high-temperature shape memory alloys based on nitix compositions for high-force actuator applications. In Proceedings of the SMST-2006—International Conference on Shape Memory and Superelastic Technologies, Pacific Grove, CA, USA, 7–11 May 2006; pp. 787–802. [CrossRef]
32. Wu, Z.; Benafan, O.; Lawson, J.W. A first-principles study of the phase transitions in ultrahigh temperature shape memory alloy RuNb. *Acta Mater.* **2024**, *276*, 120140. [CrossRef]
33. Krooß, P.; Niendorf, T.; Kadletz, P.M.; Somsen, C.; Gutmann, M.J.; Chumlyakov, Y.I.; Schmahl, W.W.; Eggeler, G.; Maier, H.J. Functional Fatigue and Tension–Compression Asymmetry in [001]-Oriented $Co_{49}Ni_{21}Ga_{30}$ High-Temperature Shape Memory Alloy Single Crystals. *Shape Mem. Superelasticity* **2015**, *1*, 6–17. [CrossRef]
34. Exarchos, D.A.; Dalla, P.T.; Tragazikis, I.K.; Dassios, K.G.; Zafeiropoulos, N.E.; Karabela, M.M.; De Crescenzo, C.; Karatza, D.; Musmarra, D.; Chianese, S.; et al. Development and characterization of high performance Shape Memory Alloy coatings for structural aerospace applications. *Materials* **2018**, *11*, 832. [CrossRef] [PubMed]